Selection rules and line strengths of Zeeman-split dark resonances

R. Wynands, A. Nagel, S. Brandt, D. Meschede, and A. Weis

Institut für Angewandte Physik, Universität Bonn, Wegelerstraße 8, 53115 Bonn, Germany

In a weak magnetic field coherent dark resonances in cesium vapor are split into up to 15 resolved components, depending on field direction and laser polarizations. We find that the selection rules are different for vapor cells with and without buffer gas due to a change in multipolarity of the two-photon coupling. At low laser intensities or sufficiently high buffer-gas pressure optical pumping between different dark resonances can be neglected so that a simple model allows one to calculate the relative line strengths, giving complete agreement with the experimental spectra. [S1050-2947(98)00907-X]

PACS number(s): 32.70.Cs, 32.60.+i, 42.50.Gy, 32.70.Fw

I. INTRODUCTION

Dark resonances can occur when two coherent light fields couple two atomic levels to a common third level. A particularly useful system for the observation of such resonances is provided by the vapors of the alkali metals, where the two hyperfine-split ground levels can be coupled to the first excited level by two light fields resonant with a D line. This arrangement of levels is called a Λ configuration. When the laser difference frequency matches the ground-state splitting, the atomic population is optically pumped into a coherent superposition of the two lower states with a phase such that absorption of the optical fields vanishes. This coherence has a very long radiative lifetime because a direct transition between the two ground states is electric dipole forbidden, which leads to potentially very narrow resonance lines. In practice, the linewidth is determined by laser difference frequency jitter and time-of-flight, collisional, and power broadening.

In a real atom the pure three-level case is rarely realized. In the case of cesium, for instance, which was used in the experiments described here, a total of 32 levels are involved in the D_1 line and 48 levels in the D_2 line. In a weak magnetic field these levels are Zeeman shifted and in general different Λ systems with different ground-state splittings, i.e., resonance frequencies, are formed. The relative strengths of the individual resonances depend on the magnetic field direction and the light polarizations.

Since the observation of coherent dark resonances [1] the unique combination of low absorption and narrow linewidth has found many applications, among them atomic beam frequency standards [2], electromagnetically induced transparency in optically thick media [3], and laser cooling below the one-photon recoil limit [4]. These and other related activities were recently reviewed by Arimondo [5].

A particularly interesting application of coherent dark states is magnetometry, where extremely high sensitivities have been predicted [6,7]. For a practical realization of a dark state magnetometer a detailed understanding of the characteristics of coherent dark resonances in magnetic fields is essential. Except for the work on the width of the transmission window of electromagnetically induced transparency as a function of magnetic field strength [8], we do not know of any systematic experimental work on coherent dark reso-

nances in magnetic fields. In this paper we describe how symmetry arguments can be used to calculate the selection rules and the relative line strengths in such a superposition of Λ systems, both with and without the presence of a buffer gas, and compare the results to experiments on the D_2 line in cesium vapor.

II. EXPERIMENTAL SETUP

In the experiments two diode lasers resonant with the cesium D_2 transition at 852 nm are phase locked to each other with a frequency difference of 9.2 GHz, corresponding to the cesium ground-state hyperfine splitting (Fig. 1). The 9.2-GHz reference signal is provided by stable rf oscillators so that all fluctuations of the laser difference frequency are eliminated by the phase-locked loop [9]. The laser beams are superposed and copropagate through a cesium vapor cell at ambient temperature. Dark resonance widths of 30 kHz can be observed in this way, mainly limited by time-of-flight broadening [10]. Recently we have narrowed the linewidth to below 50 Hz using neon as a buffer gas [9]. In the buffer gas the free motion of the cesium atoms through the laser beams is impeded by frequent collisions with Ne atoms so that the interaction time is increased. At a neon pressure of several 10 mbar the coherence survives more than 10^7 Cs-Ne collisions (corresponding to a lifetime of milliseconds) whereas the upper state is broadened to about 1 GHz or more. This is much more than the hyperfine splitting of the $6P_{3/2}$ state so that its $F=2,3,4,5$ levels are not resolved. Since $F=2$ and $F=5$ can be reached by one-photon transitions but cannot be
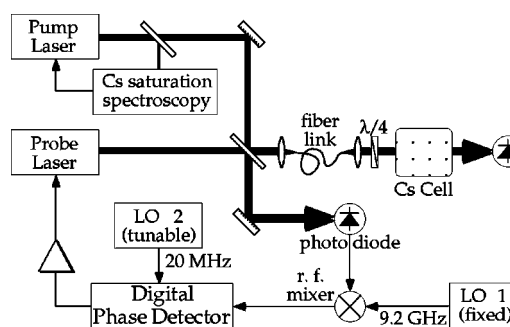

FIG. 1. Experimental setup for the observation of coherent population trapping resonances in cesium vapor.
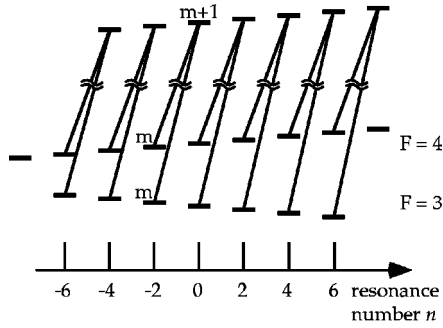
FIG. 2. Zeeman-split cesium dark resonances with $\sigma^+ \sigma^+$ excitation. Seven Λ systems are allowed by the selection rules, giving rise to seven coherent dark resonances, the positions of which are indicated by the short vertical lines. The resonances are labeled by n, the sum of the magnetic quantum numbers of the coupled lower levels. The Raman resonance frequencies are proportional to n.

part of a Λ system, the contrast of the coherent dark resonances is reduced by one-photon absorption out of the dark states. The frequent collisions also lead to a rapid depolarization of the excited states [11]. The buffer-gas pressures used in our experiment, however, are too low to cause population transfer between the $6P_{3/2}$ and the $6P_{1/2}$ states [11].

Data are taken by scanning one laser (frequency ω_1) over the $6S_{1/2}, F=3 \rightarrow 6P_{3/2}$ transition while the other laser (frequency ω_2) is kept locked to the $6S_{1/2}, F=4 \rightarrow 6P_{3/2}, F =3,4$ crossover transition of a saturated absorption spectrum in an auxiliary cell [12]. Spectra are recorded by measuring the transmitted power as a function of laser difference frequency. A typical spectrum consists of a Doppler or collisionally broadened background on which the dark resonance proper is superimposed. The zero of the frequency axis corresponds to the Raman resonance condition $\omega_1 - \omega_2 = \omega_{\text{hfs}}$, where ω_{hfs} is the frequency splitting of the $|F=3\rangle$ and the $|F=4\rangle$ ground states in zero magnetic field. In order to enhance the signal-to-noise ratio the 9.2-GHz oscillator frequency is modulated at 1 kHz with a 1-kHz amplitude and the transmission signal of the cesium vapor cell is demodulated by a dual-phase lock-in amplifier. For a spectral structure with a linewidth much larger than 1 kHz the in-phase component yields the derivative of the spectral line shape while the quadrature component vanishes, i.e., an absorption feature will look dispersionlike. In all experiments described here the intensity of the fixed frequency laser is 50% larger than that of the scanning laser.

Three mutually perpendicular pairs of current coils are used to compensate static magnetic fields inside the cesium vapor. By changing the currents in these coils small homogeneous magnetic fields can be applied in arbitrary directions. In a small longitudinal field B the $6S_{1/2}, F=3$ and $F=4$ ground states split into seven and nine magnetic substates whose frequencies are Zeeman shifted at a rate of $-\gamma B m_3$ and $\gamma B m_4$, respectively, where $\gamma = g_J \mu_B /(2I +1)h = 3.5$ kHz/μT, g_J is the electronic g factor, and μ_B the Bohr magneton (Fig. 2). m_3 and m_4 are the magnetic quantum numbers in the $F=3$ and $F=4$ ground states. For σ^+-polarized lasers the one-photon electric dipole selection rules allow the formation of seven Λ systems, each one offset in frequency from the unperturbed hyperfine frequency by $f_n = n \gamma B$ in the linear Zeeman regime where $n=m_3$

$+m_4$. Only levels with $\Delta m = 0$ are coupled in this configuration, i.e., only resonances with even n occur, as shown in Fig. 2.

III. LINE STRENGTHS: THEORETICAL MODEL

We consider the case of Λ systems involving alkali-metal-atom ground states. In weak magnetic fields the states $\{|\alpha F m_F\rangle\}$ are a suitable basis where $|\alpha\rangle$ is a shorthand notation for $|\nu L J\rangle$. The quantization direction $\hat{e}_z$ is taken along the magnetic field direction. For flux densities below 10 mT F mixing in the upper state is negligible.

For a complete description of the behavior of the atom in the presence of the two light fields one has to solve the equations of motion for the density matrix. This is a rather cumbersome calculation because of the large number of levels involved (48 levels in the worst case, the D_2 line in cesium). Many authors have solved this problem numerically (see Arimondo's review article [5] for references). The numerical solution, however, makes it hard to obtain physical insight. On the analytical side, there is a series of papers by a theoretical group that culminated in Ref. [13], where for zero magnetic field the density matrix was expanded into a series of invariant parts, valid in the case of purely radiative damping. Hioe and Carroll [14] found general invariants in multilevel quantum systems, while Kanokogi and Sakurai [15] gave another elegant approach that, however, takes only one excited level into account.

Here we present a simple and physically intuitive model that allows a quantitative description of the measured relative line strengths for all polarizations, field directions, and with or without buffer gas. The model is based on an irreducible tensor description of the interaction of the bichromatic light field with the atomic levels.

The key idea of the model is to separately consider all possible pairs of magnetic substates with one state taken from each ground-state F level. For each of those pairs $\{|\alpha_i F_i m_i\rangle, |\alpha_f F_f m_f\rangle\}$ the matrix element of an effective two-photon operator $\mathcal{O}_\Lambda$ for the transition from $|i\rangle$ to $|f\rangle$ is calculated and summed over all possible upper states and all polarization components present in the light fields. Since the contrast of the unresolved resonance lines in the unsaturated case increases with laser intensity [5], i.e., Rabi frequency, it is reasonable to assume that the total strength of the resonance is distributed among the Zeeman-split components according to the ratios of the effective Rabi frequencies for the two-photon coupling. The Rabi frequencies, in turn, contain the matrix element of the transition so that the relative strengths of the coherent dark resonance components are proportional to the square of the matrix elements

$$S_{\text{rel}}(m_i, m_f) = |A_\Lambda(m_i, m_f)|^2 \propto |\langle \alpha_f F_f m_f | \mathcal{O}_\Lambda | \alpha_i F_i m_i \rangle|^2. \tag{1}$$

Here A_Λ is the transition amplitude for the process where one photon is absorbed from one of the light beams and a second one emitted into the second light beam. In the unsaturated case discussed here the absolute laser intensities enter as proportionality factors for all components equally so that they do not have an effect on the relative line strengths.
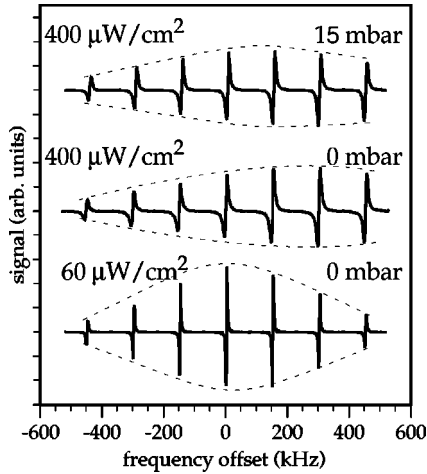
Several assumptions underlie this approach.

FIG. 3. Coherent dark resonance spectra in a longitudinal magnetic field for $\sigma^+\sigma^+$ excitation. The asymmetry of the middle spectrum is due to optical depopulation pumping. The spectrum becomes symmetric when the laser intensity is reduced (bottom) or the neon buffer-gas pressure is increased (top). For higher intensities the individual lines are power broadened (top and middle traces).

(i) The shape of a dark resonance spectrum in a magnetic field is influenced by optical pumping. When both lasers are σ^+ polarized the atomic population is preferentially transferred to levels with large m quantum numbers (middle trace in Fig. 3). For lower laser powers the pumping rate is reduced, resulting in a more symmetric spectrum (bottom trace). At the same time the individual peaks become narrower because of reduced power broadening.

Alternatively, optical pumping can be suppressed and the spectrum symmetrized by increasing the buffer-gas pressure (top trace). Buffer-gas collisions reduce the pumping efficiency through two mechanisms: The homogeneous linewidth is increased to several hundred megahertz or more, which directly reduces the pumping rate, and the excited state is depolarized, which causes a redistribution of the population over all ground states. For sufficiently low laser power and high buffer-gas pressure optical pumping therefore can be neglected, which greatly simplifies the calculation of relative line strengths.

(ii) In the case of alkali-metal-atom D_2 lines the excited states $F = I \pm 3/2$ cannot couple to *both* ground states simultaneously. These levels therefore form a loss channel for the coherent state through one-photon absorption. In general, the one-photon transition rates are different for different coherent states and can change the population balance between the coherent dark states. This one-photon loss mechanism is also ignored.

(iii) Depending on experimental parameters, some sublevels of the ground state can simultaneously be coupled to more than one other ground-state sublevel. In this simple model we ignore all interference effects (i.e., coherences involving more than two photons) due to shared levels among pairs of ground states. Initially this assumption seems unfounded. However, the comparison with experimental results shows that it is indeed justified.

A. Two-photon matrix element

Following the treatment in [16] for two-photon absorption, the two-photon Λ transition amplitude A_Λ can be de-

rived in second-order perturbation theory for stimulated two-photon Λ processes. When keeping only resonant terms one obtains

$$A_\Lambda \propto \sum_s \frac{\langle f|\vec{d}\cdot\vec{E}_2^*|s\rangle\langle s|\vec{d}\cdot\vec{E}_1|i\rangle}{\omega_1 - \omega_{si} + i\Gamma_s/2} \qquad (2)$$

$$\propto \sum_s \sum_{p,q} (-1)^{p+q} a_{-p}b_{-q} \frac{\langle f|r_q|s\rangle\langle s|r_p|i\rangle}{\omega_1 - \omega_{si} + i\Gamma_s/2}. \qquad (3)$$

Here $\vec{r}$ is the position operator of the valence electron, $|s\rangle$ are all possible intermediate excited states, ω_1 is the frequency of the light field $\vec{E}_1$, ω_{si} is the frequency difference between states $|s\rangle$ and $|i\rangle$, and Γ_s is the dephasing rate of state $|s\rangle$. The electric light fields have been written as standard tensor components

$$\vec{E}_1 = a_1\hat{e}_1 + a_0\hat{e}_0 + a_{-1}\hat{e}_{-1}, \qquad (4)$$

$$\vec{E}_2^* = (\tilde{b}_1\hat{e}_1 + \tilde{b}_0\hat{e}_0 + \tilde{b}_{-1}\hat{e}_{-1})^* \qquad (5)$$

$$= -(\tilde{b}_{-1})^*\hat{e}_1 + (\tilde{b}_0)^*\hat{e}_0 - (\tilde{b}_1)^*\hat{e}_{-1} \qquad (6)$$

$$=: b_1\hat{e}_1 + b_0\hat{e}_0 + b_{-1}\hat{e}_{-1}, \qquad (7)$$

so that

$$\vec{d}\cdot\vec{E}_1 = -|e| \sum_{p=-1}^{1} (-1)^p a_{-p}r_p. \qquad (8)$$

For example, in the case of the cesium D_2 line discussed here, $|i\rangle = |6S_{1/2}, F=3, m_3\rangle$, $|f\rangle = |6S_{1/2}, F=4, m_4\rangle$, and $|s\rangle = |6P_{3/2}, F_s, m_s\rangle$.

Equation (3) can be written as

$$A_\Lambda \propto \sum_{K=0}^{2} \sum_{Q=-K}^{K} (-1)^Q a_{-Q}^{(K)}\langle f|R_Q^{(K)}|i\rangle, \qquad (9)$$

with

$$a_Q^{(K)} = \sum_{p,q} \langle 1p1q|KQ\rangle a_p b_q, \qquad (10)$$

$$R_Q^{(K)} = \sum_s \sum_{p,q} \langle 1p1q|KQ\rangle(r_p|s\rangle\langle s|r_q)/N(s), \qquad (11)$$

$$N(s) = \omega_1 - \omega_{si} + i\Gamma_s/2. \qquad (12)$$

Here $a_Q^{(K)}$ depends only on the laser polarizations and $R_Q^{(K)}$ contains only atomic quantities.

Application of the Wigner-Eckart theorem to $\langle f|R_Q^{(K)}|i\rangle$ allows one to split off the Q dependence

$$A_\Lambda \propto (-1)^{F_f - m_f} \sum_{K,Q} (-1)^Q a_{-Q}^{(K)} \begin{pmatrix} F_f & K & F_i \\ -m_f & Q & m_i \end{pmatrix} \mathcal{M}^{(K)}, \qquad (13)$$

where

$$\mathcal{M}^{(K)}=(-1)^{F_i-F_f+K}\sqrt{2K+1}\sum_{\alpha,F_s}(-1)^{2F_s}\begin{Bmatrix}F_f & K & F_i\\ 1 & F_s & 1\end{Bmatrix}$$

$$\times\langle F_f||r||F_s\rangle\langle F_s||r||F_i\rangle/N(\alpha,F_s)\qquad(14)$$

is the multipole amplitude of the coupling with multipolarities $K=0,1,2$ corresponding to scalar, vector, and quadrupole couplings. For coherent dark resonances in alkali-metal-atom ground states, where $F_f\neq F_i$, the $3j$ symbol in Eq. (13) vanishes for $K=0$: Scalar coupling is not possible. From Eq. (13) one also sees immediately that for each pair of initial and final states the sum (9) reduces to the two terms with $Q=m_f-m_i$:

$$S_{\text{rel}}\propto|a_{-Q}^{(1)}\langle f|R_Q^{(1)}|i\rangle+a_{-Q}^{(2)}\langle f|R_Q^{(2)}|i\rangle|^2.\qquad(15)$$

For the case of two-photon absorption a similar separation into a sum of tensor products was discussed by Cagnac *et al.* [17] for the case $\omega_1=\omega_2$ and by Herrmann *et al.* [18] for $\omega_1\neq\omega_2$. The polarization-dependent part was also derived by Bonin and McIlrath [19] in order to study selection rules for two-photon absorption. Yuratich and Hanna [20] found a general expression for multiphoton processes of arbitrary order, based on symmetry arguments, and discussed Raman transitions as a special case.

A nonzero element $a_{-Q}^{(K)}$ means that coherences between ground states with $m_f-m_i=Q$ are allowed, provided $\mathcal{M}^{(K)}$ and the $3j$ symbol do not vanish. $\mathcal{M}^{(K)}$ can be written as the product of a term $\mathcal{V}(K,F_s)$ depending on F_s and a term $\mathcal{U}(K)$ containing the F_s-independent terms:

$$\mathcal{M}^{(K)}=\mathcal{U}(K)\sum_{\alpha,F_s}\mathcal{V}(K,F_s),\qquad(16)$$

$$\mathcal{U}(K)=(-1)^{I+L_f+S_f+J_s+L_s+S_s}(2J_s+1)[(2K+1)(2F_f+1)$$

$$\times(2F_i+1)(2J_f+1)(2J_i+1)]^{1/2}\qquad(17)$$

$$\times\begin{Bmatrix}L_f & J_f & S_f\\ J_s & L_s & 1\end{Bmatrix}\begin{Bmatrix}L_s & J_s & S_s\\ J_i & L_i & 1\end{Bmatrix}\langle L_f||r||L_s\rangle$$

$$\times\langle L_s||r||L_i\rangle,\qquad(18)$$

$$\mathcal{V}(K,F_s)=\frac{(-1)^{F_i+F_s+F_f+I+J_i+J_s+J_f+K}}{N(\alpha,F_s)}\begin{Bmatrix}F_f & F_s & 1\\ 1 & K & F_i\end{Bmatrix}$$

$$\times\begin{Bmatrix}I & F_s & J_s\\ 1 & J_f & F_f\end{Bmatrix}\begin{Bmatrix}F_i & F_s & 1\\ J_s & J_i & I\end{Bmatrix}.\qquad(19)$$

At sufficiently high buffer-gas pressure Γ_s dominates the resonance denominator $N(\alpha,F_s)$ in Eq. (19), making it effectively independent of F_s. Then the sum over $6j$ symbols can be evaluated explicitly:

$$\sum_{F_s}\mathcal{V}(K,F_s)=\begin{Bmatrix}J_i & K & J_f\\ F_f & I & F_i\end{Bmatrix}\begin{Bmatrix}J_i & K & J_f\\ 1 & J_s & 1\end{Bmatrix}\frac{1}{N(\alpha)}.$$
$$(20)$$

For coherent dark resonances in alkali-metal-atom ground states one has $S_f=S_s=S_i=1/2$, $F_f=F_i+1$, $F_i=I-1/2$, $J_f=J_i=1/2$, and $J_s=1/2$ or $3/2$, so that
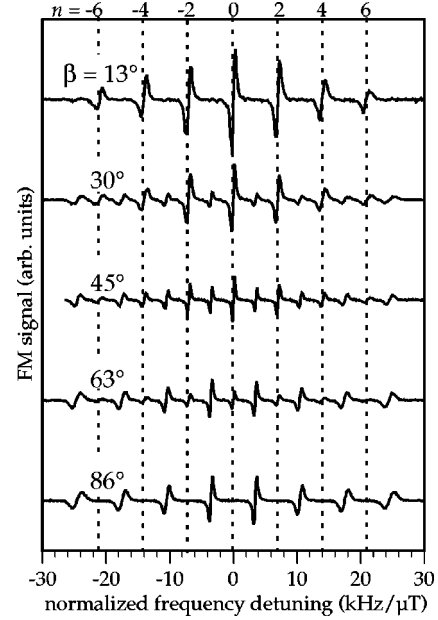

FIG. 4. Coherent dark resonance spectra for $\sigma^+\sigma^+$ excitation and different angles β between the laser beam and external magnetic field. There is a smooth transition from a spectrum with 7 peaks via 15 peaks to 8 peaks (87 mbars of Ne buffer gas).

$$\sum_{F_s}\mathcal{V}(1,F_s)=(-1)^{2I+J_s+1/2}\frac{J_s(J_s+1)-11/4}{18(2I+1)}\frac{1}{N},\quad(21)$$

$$\sum_{F_s}\mathcal{V}(2,F_s)=0.\qquad(22)$$

For $K=2$ the triangle conditions in each $6j$ symbol are violated: In a buffer gas no quadrupole coupling is possible. $K=2$, however, is allowed for low buffer-gas pressure where the more general equation (19) has to be used, making it interesting to study the multipolarity of the coupling as a function of buffer-gas pressure (see Sec. IV C). This can be understood intuitively when the ratio of the two terms making up the sum in Eq. (19) ($F_s=F_i$, $F_s=F_i+1$) is calculated,

$$\frac{\mathcal{V}(1,F_s=F_i)}{\mathcal{V}(1,F_s=F_i+1)}=\frac{I-1/2}{I+3/2}\frac{N(F_i+1)}{N(F_i)},\qquad(23)$$

$$\frac{\mathcal{V}(2,F_s=F_i)}{\mathcal{V}(2,F_s=F_i+1)}=-\frac{N(F_i+1)}{N(F_i)},\qquad(24)$$

independently of J_s. Equation (24) shows that, except for the resonance denominators, both excited-state F levels contribute to the quadrupole coupling with equal amplitude but opposite sign, thus gradually canceling out the $K=2$ coupling for increasing buffer-gas pressure. In contrast, the vector coupling in general survives. A similar argument was given by Happer and Mathur [21] for the case of one-photon optical pumping of atoms with a hyperfine splitting smaller than the Doppler broadening.

B. Magnetic-field direction

When a magnetic field is applied in the x-z plane at an angle β with respect to the propagation direction of the light beams the input polarizations have to be transformed into a coordinate system with $\hat{e}_z$ along $\vec{B}$ using the rotation matrices $D_{QQ'}^{(K)}$:

$$\tilde{a}_{Q'}^{(K)} = \sum_Q a_Q^{(K)} D_{QQ'}^{(K)}. \tag{25}$$

Let us look at the specific example where both light beams are σ^+ polarized with respect to a magnetic field along their propagation direction. In this case the only nonzero components of $a_Q^{(K)}$ have $Q = m_f - m_i = 0$:

$$a_0^{(2)} = -\frac{1}{\sqrt{6}}, \quad a_0^{(1)} = -\frac{1}{\sqrt{2}}, \quad a_0^{(0)} = -\frac{1}{\sqrt{3}}. \tag{26}$$

For $\beta \neq 0$ the polarization tensor components are

$$\tilde{a}_2^{(2)} = -\frac{1}{4}\sin^2 \beta,$$

$$\tilde{a}_1^{(2)} = -\frac{1}{4}\sin 2\beta, \quad \tilde{a}_1^{(1)} = -\frac{1}{2}\sin \beta,$$

$$\tilde{a}_0^{(2)} = \frac{1}{\sqrt{6}}\left(\frac{3}{2}\sin^2 \beta - 1\right), \quad \tilde{a}_0^{(1)} = -\frac{1}{\sqrt{2}}\cos \beta,$$

$$\tilde{a}_0^{(0)} = -\frac{1}{\sqrt{3}}, \tag{27}$$

$$\tilde{a}_{-1}^{(2)} = \frac{1}{4}\sin 2\beta, \quad \tilde{a}_{-1}^{(1)} = \frac{1}{2}\sin \beta,$$

$$\tilde{a}_{-2}^{(2)} = -\frac{1}{4}\sin^2 \beta.$$

For $\beta = 0°$ only the $Q=0$ components do not vanish so that only even-numbered peaks are allowed; this is the situation depicted in Fig. 2. For $\beta = 90°$ all 15 possible components are present in a cell without buffer gas, while in a buffered cell, where $K=2$ does not occur, only odd-numbered peaks ($|Q|=1$) remain.

The transition rates vary with the square of the probability amplitudes and in the special case considered here one obtains for S_{rel}

$$S_{rel} \propto \left| -\frac{1}{\sqrt{2}}\cos \beta \langle f|R_0^{(1)}|i\rangle + \frac{1}{\sqrt{6}}\left(\frac{3}{2}\sin^2 \beta - 1\right) \right.$$

$$\left. \times \langle f|R_0^{(2)}|i\rangle \right|^2 \quad \text{for} \quad Q=0, \tag{28}$$

$$S_{rel} \propto \left| \frac{1}{2}\sin \beta \langle f|R_{\pm 1}^{(1)}|i\rangle - \frac{1}{4}\sin 2\beta \langle f|R_{\pm 1}^{(2)}|i\rangle \right|^2$$

$$\text{for} \quad Q=\pm 1. \tag{29}$$

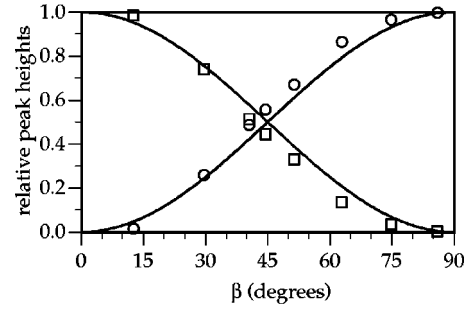In the limit of high buffer-gas pressure the $K=2$ terms become negligible:

FIG. 5. Measured resonance strengths for the seven "longitudinal" peaks (squares) and the eight "transverse" peaks (circles) (cf. Fig. 4), normalized to the total strength of all resonances. The solid lines correspond to $\sin^2 \beta$ and $\cos^2 \beta$, where β is the angle between the field and laser propagation directions.

$$S_{rel} \propto \cos^2 \beta \quad \text{for} \quad Q=0, \tag{30}$$

$$S_{rel} \propto \sin^2 \beta \quad \text{for} \quad Q=\pm 1. \tag{31}$$

The strengths of the even-numbered resonances are therefore expected to decrease as $\cos^2 \beta$, while those of odd-numbered resonances should increase as $\sin^2 \beta$.

IV. LINE STRENGTHS: EXPERIMENTAL TESTS

A. Magnetic-field direction

The angular dependence of Eqs. (30) and (31) is illustrated in Fig. 4 with a series of spectra recorded with identical circular laser polarizations in a cell with 87 mbars of neon buffer gas. At such a high pressure only the $K=1$ com-
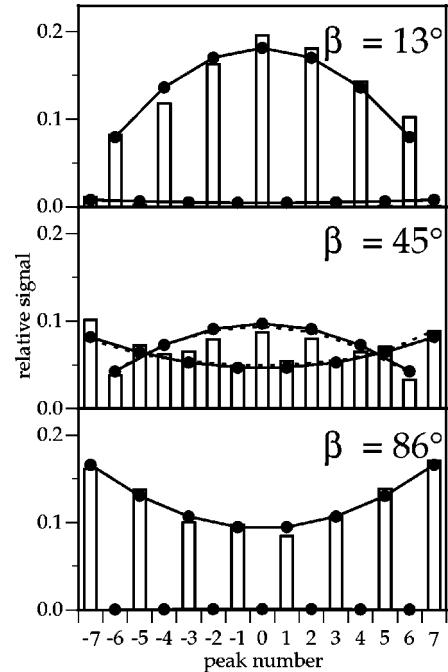

FIG. 6. Comparison of calculated (dots) and measured (columns) resonance strengths for selected spectra of Fig. 4. The column heights reflect the strengths of the experimental peaks, while the dots (solid lines) indicate the results of a calculation in the limit of high buffer-gas pressure. The dashed lines correspond to a complete calculation using Eq. (13) with $\Gamma_s = 2\pi \times 300$ MHz.
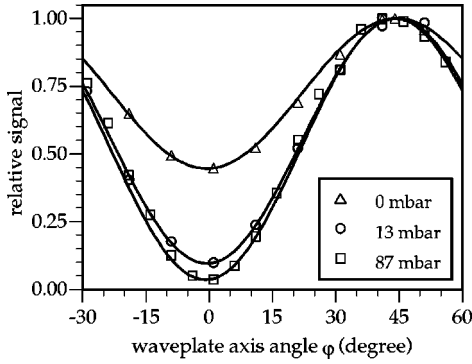
FIG. 7. Dependence of resonance strength on laser polarization in a buffer-gas cell and zero magnetic field. $\varphi = 45°$, circular polarization; $\varphi = 0°$, linear polarization. The solid lines are numerical fits with a $\sin^2 2\varphi$ dependence on top of a constant offset.

ponent of the coupling effectively survives. When the angle β in the x-z plane is increased the seven even-numbered resonances seen at low β gradually vanish, while the eight odd-numbered resonances continually grow until, for large β, they alone make up the spectrum. The broadening of the lines toward the outer peaks is due to field inhomogeneities.

For a quantitative comparison with theory one has to determine the total strength of each component. This was done by performing a ''running sum'' on the raw spectra in Fig. 4, i.e., for each frequency the intensities of all data points to the left of it are summed. The result is a series of lines with absorptive shapes whose areas can be determined by integration. This area is taken as a measure of the relative line strengths.

The $\sin^2 \beta$ and $\cos^2 \beta$ dependences for the line strengths of odd- and even-numbered resonances were checked using eight spectra for different β, five of which are shown in Fig. 4. For each β the sum S_{even} of the strengths S_{2i} of the seven even-numbered resonances and the sum S_{odd} of the eight odd-numbered resonances S_{2i+1} were normalized to the total strength $S = S_{\text{even}} + S_{\text{odd}}$ (squares and circles in Fig. 5). The solid line represents the pure $\cos^2 \beta$ and $\sin^2 \beta$ dependences anticipated from Eqs. (30) and (31).

While there is qualitative agreement, there are systematic differences: The squares are mostly too low and the circles too high. Such a systematic deviation could be due to an additional magnetic field component in the y direction.

B. Relative line strengths in buffered cells

If the buffer-gas pressure is high enough (greater than 10 mbars of neon for the cesium D_2 line) the resonance denominators $N(F_s)$ are mainly determined by the collisionally increased Γ_s, as discussed above. It is therefore possible to simplify the calculations by treating $N(F_s)$ as a constant and by omitting it from Eq. (3) for a calculation of relative line strengths. The results of a numerical calculation for circular light polarizations are shown in Fig. 6 as dots connected by solid lines. For completeness the results of the full calculation using Eq. (13) including the resonance denominators $N(F_s)$ with $\Gamma_s = 2\pi \times 300$ MHz are shown as dashed lines. Γ_s was estimated from a Voigt profile fit to a Doppler and collisionally broadened optical transmission profile. The experimental and theoretical spectra have each been normal-
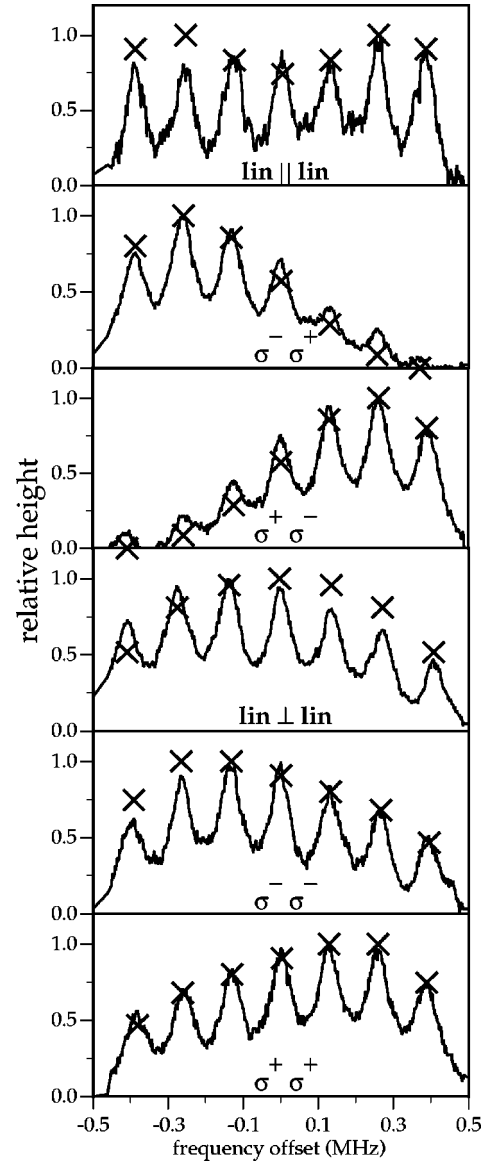

FIG. 8. Polarization dependence of line strengths in a cesium cell without buffer gas (crosses, theoretical values). The highest peak in each experimental and theoretical spectrum was normalized to unity. The experimental data were taken from [22].

ized to the unit total line strength. The good agreement justifies our omission in the theoretical model of interaction effects between different Λ systems with shared lower levels.

In the raw data for $\beta = 86°$ the outermost lines seem very weak (Fig. 4), while in reality they are the strongest components (columns in Fig. 6). This effect is due to field inhomogeneities that broaden the lines at the expense of their heights while leaving the peak areas constant.

C. Change of multipolarity

The circular polarization used to record the spectra shown in the previous figures is produced with a quarter-wave plate whose axis is aligned along the x axis. The direction of the linear input polarization makes an angle of $\varphi = 45°$ with the x axis. When φ is reduced from $45°$ to $0°$ the polarization gradually changes from circular to linear:

$$\vec{p} = (\cos \varphi)\hat{e}_x + i(\sin \varphi)\hat{e}_y \qquad (32)$$

$$= (\cos \varphi - \sin \varphi)\hat{e}_x - \sqrt{2}(\sin \varphi)\hat{e}_1 \qquad (33)$$

and similarly for $\vec{q}$, giving, for $a_Q^{(K)}$,

$$\tilde{a}_2^{(2)} = \frac{1}{2}\cos 2\varphi,$$

$$\tilde{a}_1^{(2)} = 0, \quad \tilde{a}_1^{(1)} = 0,$$

$$\tilde{a}_0^{(2)} = -\frac{1}{\sqrt{6}}, \quad \tilde{a}_0^{(1)} = \frac{1}{\sqrt{2}}\sin 2\varphi, \quad \tilde{a}_0^{(0)} = -\frac{1}{\sqrt{3}}, \quad (34)$$

$$\tilde{a}_{-1}^{(2)} = 0, \quad \tilde{a}_{-1}^{(1)} = 0,$$

$$\tilde{a}_{-2}^{(2)} = \frac{1}{2}\cos 2\varphi.$$

In a buffer gas, where only $K=1$ contributes, the line strength should thus depend on φ like $\sin^2 2\varphi$. This was checked experimentally in three cesium cells with 0, 13, and 87 mbars of Ne at zero magnetic field. In Fig. 7 the total area of the dark resonance is plotted as a function of φ. The solid lines are numerical fits of a $A + (1-A)\sin^2 2\varphi$ dependence.

From the fit one obtains $A = 0.45$, 0.095, and 0.036 for pressures 0, 13, and 87 mbars, respectively. This confirms the gradual change in multipolarity predicted by Eqs. (23) and (24) and might be a way to determine Γ_s as a function of pressure without actually having to measure lifetimes or detailed line shapes.

D. Cell without buffer gas

In a vapor cell at room temperature the Doppler width of the cesium D_2 line is 370 MHz, which is comparable to the hyperfine splittings of 251, 202, and 151 MHz in the $6P_{3/2}$ state. If the laser frequencies are tuned into the hyperfine manifold of the $6P_{3/2}$ state there is, for each level $|F_s\rangle$, a velocity class that is resonant with the transition $|i\rangle \rightarrow |s\rangle$. This class with a width corresponding to the homogeneous width Γ_s will give the dominant contribution of level $|F_s\rangle$ to the line strength. If the states $|s\rangle$ have a frequency difference larger than Γ_s, for each individual atom only one level $|F_s\rangle$ will effectively enter into S_{rel} because for the other level the

optical detuning is too large. In effect, there are no atoms that give contributions for both values of F_s, so that the relative signs of the contributions are irrelevant and one can sum over rates instead of amplitudes. The calculation of S_{rel} can therefore be simplified by performing an incoherent summation over F_s and by once again omitting $N(F_s)$ (thus assuming equal numbers of atoms in each relevant velocity class):

$$S_{\text{rel}} = \sum_{F_s} \left| \sum_{K,Q} (-1)^Q a_{-Q}^{(K)} \begin{pmatrix} F_f & K & F_i \\ -m_f & Q & m_i \end{pmatrix} \mathcal{U}(K)\mathcal{V}(K,F_s) \right|^2. \qquad (35)$$

In this way the power-broadened spectra for various polarization configurations that were measured in our laboratory [22] in a cell without buffer gas can also quantitatively be reproduced (Fig. 8). Small deviations between experiment and theory can be explained by an imperfect quarter-wave plate. The upper three spectra in Fig. 8 correspond to pure quadrupole coupling ($K=2$); in cells with buffer gas no spectra can be seen for these polarization configurations. The lower three spectra in Fig. 8 have both $K=1$ and $K=2$ contributions. This is the reason why the relative line strengths here are different from the spectra for the $\sigma^+\sigma^+$ configuration in buffer-gas cells (see Fig. 3) where only $K=1$ contributes.

V. CONCLUSION

We have developed an analytical model for the relative line strengths in coherent dark resonances in multilevel Λ systems. This model is valid for low light intensities or high buffer-gas pressures when optical pumping between different Λ systems can be neglected. We find good agreement with our experimental data on the cesium D_2 line. For the case of alkali-metal atoms the calculations can be simplified for the special cases without buffer gas and of high buffer-gas pressure. The spectral features observed for different field orientations, polarizations, and buffer-gas pressures were traced back to multipole orders of an effective coherent two-photon coupling between the lower states of the Λ system.

[1] G. Alzetta, A. Gozzini, L. Moi, and G. Orriols, Nuovo Cimento B **36**, 5 (1976).

[2] J. E. Thomas, P. R. Hemmer, S. Ezekiel, C. C. Leiby, Jr., R. H. Picard, and C. R. Willis, Phys. Rev. Lett. **48**, 867 (1982).

[3] K.-J. Boller, A. Imamoğlu, and S. E. Harris, Phys. Rev. Lett. **66**, 2593 (1991).

[4] A. Aspect, E. Arimondo, R. Kaiser, N. Vansteenkiste, and C. Cohen-Tannoudji, Phys. Rev. Lett. **61**, 826 (1988).

[5] E. Arimondo, Prog. Opt. **35**, 257 (1996).

[6] M. O. Scully and M. Fleischhauer, Phys. Rev. Lett. **69**, 1360 (1992).

[7] M. Fleischhauer and M. O. Scully, Phys. Rev. A **49**, 1973 (1994).

[8] D. J. Fulton, R. R. Moseley, S. Sheperd, B. D. Sinclair, and M. H. Dunn, Opt. Commun. **116**, 231 (1995).

[9] S. Brandt, A. Nagel, R. Wynands, and D. Meschede, Phys. Rev. A **56**, R1063 (1997).

[10] O. Schmidt, R. Wynands, Z. Hussein, and D. Meschede, Phys. Rev. A **53**, R27 (1996).

[11] W. Happer, Rev. Mod. Phys. **44**, 169 (1972).

[12] O. Schmidt, K.-M. Knaak, R. Wynands, and D. Meschede, Appl. Phys. B: Lasers Opt. **59**, 167 (1994).

[13] A. V. Taichenachev, A. M. Tumaikin, and V. I. Yudin, Zh. Eksp. Teor. Fiz. **110**, 1727 (1996) [JETP **83**, 949 (1996)].

[14] F. T. Hioe and C. E. Carroll, Phys. Rev. A **37**, 3000 (1988).

[15] H. Kanakogi and K. Sakurai, Phys. Rev. A **54**, 2334 (1996).

[16] R. Loudon, *The Quantum Theory of Light* (Oxford University Press, Oxford, 1983).

[17] B. Cagnac, G. Grynberg, and F. Biraben, J. Phys. (Paris) **34**, 845 (1973).

[18] P. P. Herrmann, J. Hoffnagle, N. Schlumpf, V. L. Telegdi, and A. Weis, J. Phys. B **19**, 1271 (1986).

[19] K. D. Bonin and T. J. McIlrath, J. Opt. Soc. Am. B **1**, 52 (1984).

[20] M. A. Yuratich and D. C. Hanna, J. Phys. B **9**, 729 (1976).

[21] W. Happer and B. S. Mathur, Phys. Rev. **163**, 12 (1967).

[22] O. Schmidt, Ph.D. thesis, Universität Hannover, 1995 (unpublished).